CHAPTER IV

Schiff Base Complexes of Manganese(III) and Iron(lII). Syntheses, Structure, Polymorphism, Spectral and Magnetic Studies of $[Mn(Salpn)NCS]_2$, $[Mn(SaIpn)NCS]_n$ and $Fe(Salpn)(CH_3OH)NCS$

The combination of a pseudo-halide ion and a tetradentate Schiff base (SB) ligand is suitable for making neutral M(III) complexes of the type M(SB)X. The pseudo-halide ions, N3", NCS", NCO" have been studied extensively for their ability to bridge paramagnetic moieties into dimers, polymers and clusters.[1] These ions, especially N_3^- exhibit different bridging modes, *viz.*, μ-(1,3),[2-5] μ-(1,1),[6-9] and rarely μ-(1,1,1).[10] In the case of N3", the latter two modes are found to lead to ferromagnetic interactions. There are very few structurally characterized complexes of M(I1I) with pseudo halide bridges, where M = Mn(III),[5,11-13] Fe(III),[9,12] and Cr(III)[14]. $Mn(acac)_2X$ is found to have a linear chain structure when X is azide or thiocyanate.[5,15] Mn(salen)X is also believed to have a similar structure based on spectral and magnetic studies,[16] but there is no crystallographic data available for these complexes. Mn(salen)NCS which has been structurally characterized before, has a monomeric structure.[17] Being more flexible than salen, salpn allows both equatorial and *cis*-octahedral modes of ligation. The structure and magnetic properties of Mn(salpn)N3 and Fe(salpn)N3 have been previously reported.[12] A compound with empirical formula Mn(salpn)NCS and its hydrate have been previously prepared but not crystallographically characterized.[18] Further, the catalytic

efficiency of this compound towards epoxidation of alkenes has been investigated.[19] A recent paper by Miyasaka et al.,[20] reports magnetic and crystallographic characteristics of several substituted SB complexes of Mn(III) with halides and pseudohalides. The crystallographic characterization of Mn(salpn)NCS has been done in our laboratory previously.[21] While working with these thiocyanate complexes of Mn(III) with salpn, polymorphism has also been observed. Now, the polymorphism has been studied in detail along with its spectral and magnetic properties. Similar observations are noted with Fe(III) also. In this chapter, for the sake of completeness in the discussion, the structural details of the two polymorphic forms of Mn(salpn)NCS are presented and the results of polymorphism, spectral and magnetic studies are discussed in detail. Attempts to prepare analogous Fe(III) complexes led to the formation of Fe(salpn)(CH_3OH)NCS. Its crystal structure and spectral properties are presented.

4.1. Experimental

4.1.1. Synthesis

(a) [Mn(saIpn)NCS]2 (1): In a beaker open to the atmosphere, salicylaldehyde (0.229g 1.88 mmol) and 1,3-diaminopropane (0.071g, 0.96 mmol) were stirred into 40 mL of ethanol. $Mn(CH_3CO_2)_2{\cdot}4H_2O$ (0.245g, 1.00 mmol) was added, and the stirring continued for about 1 h. To the resulting solution, KNCS (0.200g, 2.06 mmol) dissolved in a minimum amount of water was added. The solution was allowed to stand for about 3 h to complete the air oxidation of Mn(II). The filtered solution was then kept aside at room temperature (~35 ºC) for 2-3 days over which time dark green crystals deposited. Yield: 0.330g (0.84 mmol, 89 %). Anal. Calcd. for $MnC_{18}H_{16}N_3O_2S$: C, 54.96; H, 4.10; N, 10.68. Found: C, 54.48; H, 4.13; N, 10.70. Important IR absorptions (cm^{-1}): 2043, 1601,

1543, 1468, 1443, 1396, 1310, 1148, 1124, 1076, 1030, 977, 895, 804, 754, 613, 463. When the ambient temperature was lower (18-20 °C, for example in winter) the solution affords small amounts of the polymeric form along with the dimer. Recrystallization from acetonitrile gives pure dimer over a wide range of temperatures (5-30 °C).

(b) $[Mn(salpn)NCS]_n$ (2): The procedure is the same as that for the dimer described above, except that the final solution was kept in a refrigerator (5 °C) for 8-10 days. The yield of dark green crystals of the polymer in a typical experiment was 85%. Anal. Calcd. for $MnC_{18}H_{16}N_3O_2S$: C, 54.96; H, 4.10; N, 10.68. Found: C, 54.63; H, 4.38; N, 10.65. Important IR absorptions (cm^{1}): 2068, 1609, 1541, 1466, 1400, 1300, 1150, 1 126, 1067, 1028, 968, 903, 804, 750, 615, 459.

(c) Preparation of $Fe(salpn)(CH_3OH)NCS$ (3): In a beaker open to the atmosphere, salicylaldehyde (0.229g, 1.88 mmol) and 1,3-diaminopropane (0.071 g, 0.96 mmol) were stirred into 40 mL of methanol. $Fe(ClO_4)_3 \cdot H_2O$ (0.355g, 1.00 mmol) in 17 mL methanol was added, and the stirring continued for about 15 minutes. To the resulting solution, KNCS (0.195g, 2.01 mmol) dissolved in 15 mL methanol was added and stirring continued for further 15 minutes. The final solution was filtered and refrigerated. Dark brown crystals separated after about two weeks. Yield: 0.285g (0.67 mmol, 71 %). Anal. Calcd. for $FeC_{19}H_{20}N_3O_3S$: C, 53.53; H, 4.73; N, 9.86. Found: C, 52.59; H, 4.05; N, 9.61. Important IR absorptions (KBr/cm^{-1}): 2043, 1609, 1545, 1470, 1443, 1400, 1290, 1205, 1150, 1126, 1069,1020,897,799,756,604. "

(d) Polymorphism: To study the effect of solvent, the dimer (1), obtained from the reaction in ethanol at RT, was recrystallized from various solvents, *viz.*, acetonitrile, dichloromethane, acetone, tetrahydrofuran, methanol and ethanol. In each case, crystallizations were done at two temperatures *viz.*, 35 °C and 5 °C. The crystalline

products obtained after 8-10 days were identified as dimer, polymer or as a mixture of the two using IR spectroscopy *(vide supra).* Similarly, 3 was also recrystallized from solvents as mentioned above at both RT and LT. Differences in IR spectra show the presence of polymorphism, but as good quality single crystals are not obtained no stmctural work was undertaken.

4.1.2. Physical Measurements: IR spectra were obtained as KBr pellets using Shimadzu FT-IR 8000 spectrometer. C, H, N analysis of 1 and 2 were performed on a Perkin-Elmer 240C elemental analyzer at the University of Hyderabad, while for 3, the analysis was performed on a Perkin-Elmer 2400, CHNS/O analyzer at CSMCRI, Bhavnagar. Reflectance spectra of powder samples were measured using Shimadzu UV-3100 spectrometer equipped with ISR-3100 integrating sphere attachment. Absorption spectra in ACN were measured on a Shimadzu UV-3100 PC spectrometer. Single crystal X-ray data were collected on an Enraf - Nonius CAD4 diffractometer using graphite monochromated Mo Ka radiation for 1 and 2 at 1IT, Madras and for 3 at 1IT, Bombay. Powder diffractograms were measured using PW3710 model Philips Analytical X-ray diffractometer.

4.1.3. X-ray Crystallography: X-ray data were collected for dark colored crystals with dimensions, 0.35 x 0.30 x 0.10 mm for 1; 0.25 x 0.20 x 0.20 mm for 2; and 0.40 x 0.25 x 0.15 mm for 3 on an Enraf-Nonius CAD4 diffractometer at room temperature using graphite monochromated Mo Ka radiation. The data were corrected for Lorentz polarization effects and absorption.[22]-[23] The structures were solved by a combination of heavy atom and direct methods using SHELX-86[24] for 1 and 2 and SHELXS-97[25] for 3 and refined using SHELXL-93/SHELXL-97.[25] 2 was refined as a racemic twin. Drawings were made using ORTEP-III[26] and Rasmol 2.6.[27]

1 crystallizes in the orthorhombic system, space group $Pbca$, with 8 molecules in the unit cell. A total of 2906 reflections (2906 unique, 1741 with $F > 4\sigma F$) were collected in the θ range 2.16 to 24.95, with indices $0 < h \leq 14$, $0 < k \leq 16$, $0 < l < 22$. All the non hydrogen atoms were refined anisotropically while the ring hydrogen atoms were included in the calculated positions using a riding model. All the hydrogens were assigned fixed U_{iso} values, equal to $1.2U_{eq}$ of the parent atom. The final cycle of full matrix least squares refinement on F^2 converged with unweighted and weighted refinement factors of $R1 = 0.0523$ and $wR2 = 0.1303$ respectively. The goodness of fit (S) is 1.012 for 2906 unique reflections and 228 parameters. The maximum and minimum residual electron density on the final fourier map corresponded to 0.758 and -0.507 e/A^{-3} respectively.

2 crystallizes in the orthorhombic system, space group $Pna2_1$, with 4 molecules in the unit cell. A total of 3021 reflections (1551 unique, 1480 with $F > 4\sigma F$) were collected in the θ range 2.40 to 24.98, with indices $-14 < h < 14$, $0 < k < 13$, $0 < l < 13$. All the non hydrogen atoms were refined anisotropically while the ring hydrogen atoms were included in the calculated positions using a riding model. All the hydrogens were assigned fixed U_{iso} values, equal to $1.2U_{eq}$ of the parent atom. The final cycle of full matrix least squares refinement on F^2 converged with unweighted and weighted refinement factors of $R1 = 0.0219$ and $wR2 = 0.0563$ respectively. The goodness of fit (5) is 1.053 for 1543 unique reflections and 227 parameters. The maximum and minimum residual electron density on the final fourier map corresponded to 0.304 and -0.248 e/Å^{-3} respectively.

3 crystallizes in the monoclinic system, space group $C2/c$, with 8 molecules in the unit cell. A total of 4672 reflections (4382 unique, 2272 with $F > 4\sigma F$) were collected

in the grange 2.56 to 27.46, with indices $-3 < h < 21$, $-1 < k < 1$, $-34 < l < 33$. All the non hydrogen atoms were refined anisotropically while the ring hydrogen atoms were included in the calculated positions using a riding model. All the hydrogen atoms were assigned fixed U_{iso} values, equal to $1.2U_{eq}$ of the parent atom. C9 was found to be disordered and the disorder was modeled by splitting it into two halves and refined by free variable (FVAR) refinement. The final cycle of full matrix least squares refinement on F^2 converged with unweighted and weighted refinement factors of $R1 = 0.0513$ and $wR2 = 0.1136$ respectively. The goodness of fit (S) is 0.911 for 4382 unique reflections and 259 parameters. The maximum and minimum residual electron density on the final fourier map corresponded to 0.477 and -0.514 e/A^{-3} respectively.

Crystallographic data for 1, 2 and 3 are presented in Table 4.1, atomic parameters for 1 are tabulated in Table 4.2, for 2 in Table 4.3 and for 3 in Table 4.4 respectively.

Table 4.1 Crystallographic data for $[Mn(salpn)NCS]_2$ (1), $[Mn(salpn)NCS]_n$ (2) and $Fe(salpn)(CH_3OH)NCS$ (3).

	1	2	3
formula	$C_{18}H_{16}MnN_3O_2S$	$C_{18}H_{16}MnN_3O_2S$	$C_{19}H_{20}FeN_3O_3S$
formula weight	393.34	393.34	426.29
a (Å)	12.573(3)	12.5277(14)	16.431(3)
b (Å)	13.970(7)	11.576(2)	9.1571(13)
c (Å)	18.891(9)	11.513(2)	26.335(5)
α (°)	90	90	90
PC)	90	90	104.631(14)
γ (°)	90	90	90
	3318(2)	1669.6(4)	3833.8(11)
Z	8	4	8
Space group	*Pbca*	*Pna2*	*C2/c*
T (K)	293 (2)	293 (2)	293 (2)
λ **(A)**	0.71073	0.71073	0.71073
ρ_{calcd}(Mg/m^3)	1.575	1.565	1.477
μ (mm^{-1})	0.938	0.933	0.920
*R*1	0.0523	0.0219	0.0513
wR2	0.1303	0.0563	0.1136

weighting scheme, **1**: A = 0.0912; B =0.0000; *2:* A = 0.0411; B =0.1457; **3**: A = 0. 0639; B ~- 0.0000 (see p. vi for definitions).

Table 4.2 Atomic parameters for [Mn(salpn)NCS]2 (1).

Atom	10^4x	10^4y	10^4z	10^3U_{eq}	Atom	10^4x	10^4y	10^4z	10^3U_{eq}
Mn	1280(1)	4958(1)	320(1)	24(1)	C7	2395(4)	3162(3)	37(3)	32(1)
S	4527(1)	5908(1)	1455(1)	52(1)	C8	2210(6)	3354(5)	1257(3)	74(2)
01	1813(2)	4973(2)	-589(2)	31(1)	C9	1530(6)	3667(6)	1821(4)	81(2)
02	350(2)	5989(2)	53(2)	28(1)	C10	455(4)	4039(4)	1657(3)	48(2)
N1	2026(3)	3707(3)	532(2)	28(1)	CH	189(3)	5723(3)	1553(3)	31(1)
N2	533(3)	4952(3)	1269(2)	28(1)	C12	137(3)	6643(3)	1221(3)	32(1)
N3	2560(3)	5770(3)	783(2)	46(1)	C13	-97(4)	7459(4)	1646(3)	41(1)
Cl	2230(3)	4267(4)	-986(3)	32(1)	C14	-235(5)	8342(4)	1332(3)	51(2)
Cl	2421(4)	4427(4)	-1707(2)	43(1)	C15	-171(5)	8421(4)	620(4)	52(2)
C3	2795(4)	3683(5)	-2124(3)	52(2)	C16	37(4)	7657(3)	185(3)	32(1)
C4	3036(4)	2792(5)	-1855(3)	54(2)	C17	194(3)	6755(3)	489(3)	27(1)
C5	2870(4)	2634(4)	-1157(3)	46(1)	C18	3375(4)	5812(3)	1076(3)	37(1)
C6	2464(3)	3341(3)	-700(3)	35(1)					

Table 4.3 Atomic parameters for [Mn(salpn)NCS]$_n$ (2).

Atom	10^4x	10^4y	10^4z	10^3U_{eq}	Atom	10^4x	10^4y	10^4z	10^3U_{eq}
Mn1	153(1)	1089(1)	23(1)	25(1)	C7	-526(2)	-1177(2)	874(3)	31(1)
S1	-734(1)	-1789(1)	-2762(1)	39(1)	C8	-1712(2)	222(3)	1556(3)	34(1)
01	1308(1)	53(2)	-20(3)	38(1)	C9	-2382(2)	1128(2)	955(3)	35(1)
02	1076(1)	2119(2)	-774(2)	35(1)	C10	-1854(2)	2309(2)	925(3)	34(1)
Nl	-759(2)	-103(2)	874(2)	25(1)	CH	-972(2)	3249(2)	-594(3)	32(1)
N2	-967(2)	2363(2)	78(2)	27(1)	C12	-141(2)	3597(3)	-1384(3)	33(1)
N3	-584(2)	334(2)	-1610(2)	39(1)	C13	-302(3)	4603(3)	-2061(4)	45(1)
Cl	1268(2)	-1086(2)	-59(3)	31(1)	C14	497(3)	5050(3)	-2739(3)	50(1)
Cl	2145(3)	-1698(3)	-498(3)	43(1)	C15	1487(3)	4503(3)	-2747(3)	46(1)

Table 4.3 contd.....

C3	2123(3)	-2888(3)	-557(3)	50(1)	C16	1670(2)	3520(3)	-2102(3)	39(1)
C4	1248(3)	-3508(3)	-159(4)	52(1)	C17	864(2)	3039(2)	-1405(3)	31(1)
C5	399(3)	-2930(3)	291(3)	46(1)	C18	-654(2)	-538(3)	-2095(3)	32(1)
C6	394(2)	-1721(2)	349(3)	32(1)					

Table 4.4 Atomic parameters for Fe(salpn)(CH_3OH)NCS (3).

Atom	10^4x	10^4y	10^4z	10^3U_{eq}	Atom	10^4x	10^4y	10^4z	10^3U_{eq}
Fe	97(1)	2421(1)	1483(1)	34(1)	CH	-1652(3)	2240(6)	588(2)	68(1)
S1	2240(1)	1357(2)	627(1)	94(1)	C9A(0.66)	-1820(4)	971(8)	914(3)	53(3)
01	539(2)	4360(3)	1515(1)	43(1)	C9B(0.34)	-1394(10)	602(19)	590(6)	71(7)
02	819(2)	1844(3)	2158(1)	37(1)	C10	-1195(3)	-209(5)	1041(2)	65(1)
N1	-886(2)	3104(4)	821(1)	43(1)	CH	-45(2)	-813(4)	1720(2)	**41(1)**
N2	-417(2)	246(3)	1439(1)	39(1)	C12	730(2)	-769(4)	2133(1)	34(1)
N3	870(2)	1704(4)	1042(1)	52(1)	C13	1070(3)	-2086(4)	2361(2)	46(1)
Cl	471(2)	5374(4)	1149(2)	40(1)	C14	1800(2)	-2133(4)	2747(2)	47(1)
C2	1078(3)	6480(4)	1206(2)	49(1)	C15	2232(2)	-855(5)	2910(2)	48(1)
C3	996(3)	7594(5)	851(2)	59(1)	C16	1901(2)	477(4)	2708(2)	42(1)
C4	300(3)	7660(5)	419(2)	63(1)	C17	1139(2)	537(4)	2318(1)	33(1)
C5	-283(3)	6589(5)	347(2)	58(1)	C18	1448(2)	1557(5)	874(2)	45(1)
C6	**-215(2)**	**5411(4)**	701(1)	42(1)	03	-762(2)	3074(3)	1928(1)	41(1)
C7	-848(3)	4306(5)	**584(2)**	48(1)	C19	-1187(3)	4417(5)	1916(2)	70(1)

Site occupation factors of disordered atoms are given after the respective atom labels.

4.1.4. Magnetic Measurements: The two polymorphs 1 and 2 obtained from the reaction in ethanol were used for magnetic measurements. The purity of the polymorphs used for

magnetic studies were checked using IR and by comparing their X-ray powder diffraction patterns with those calculated[28] based on crystal structure. The samples were ground and pressed into pellets to avoid orientation effects. Magnetic data were recorded on a MPMS5 magnetometer (Quantum design Inc.) at Université Paris-Sud, France. The calibration was made at 298 K using a palladium reference sample furnished by Quantum design Inc. The magnetic susceptibility data were collected over a temperature range of 2-300 K at a magnetic field of 2000 G for the $[Mn(salpn)NCS]_n$ and 500 G for the [Mn(salpn)NCS]2 and were corrected for diamagnetism using Pascal's constants. In the case of $[Mn(salpn)NCS]_n$, the $\chi_M T$ versus T curve was fitted using the classical $S = 2$ chain law.[29] RT susceptibility of 3 was measured on a Sherwood scientific magnetic susceptibility balance. Calibration was made using $Hg[Co(NCS)_4]$ as standard at 300 K. Diamagnetic corrections were done using Pascal's constants.[30]

4.2. Results and Discussion

4.2.1. Structure of $[Mn(salpn)NCS]_n$ (2): The asymmetric unit of 2 is shown in Figure 4.1. The structure is analogous to that of the azide complex.[12] The salpn binds in the equatorial mode and thiocyanate acts as an end to end bridge. Each monomeric unit is related to its adjacent ones by a 2-fold screw axis, leading to a helix propagating along the crystallographic *c*-axis (Figure 4.2). While the gross structure is similar to that of the azide, there are significant differences in the coordination geometry. The two in-plane Mn-N distances in the azide complex were unequal which was attributed to the strain involved in the spiral formation (Table 2.1). In contrast, the thiocyanate has equal in-plane Mn-N distances. The long Mn-S bond apparently relieves any strain in the polymer

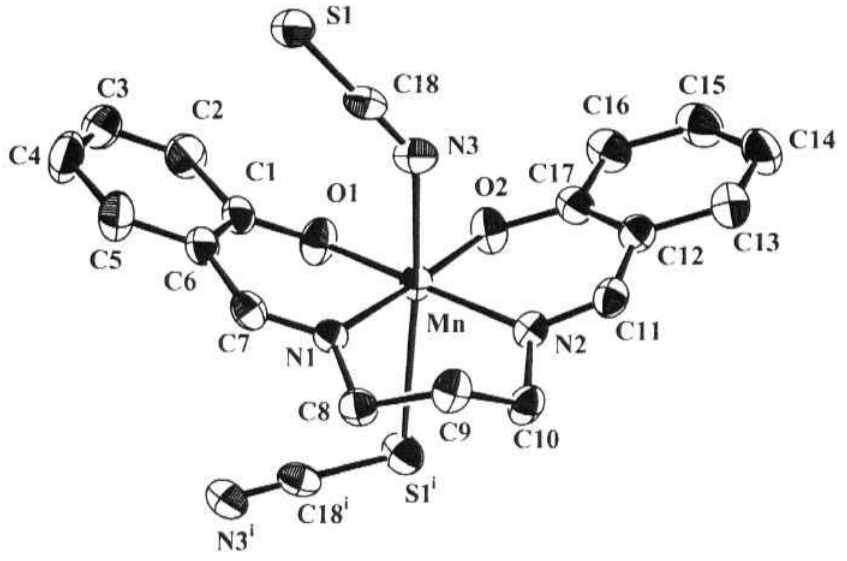

Figure 4.1 ORTEP view of one complex cation and its two bonded thiocyanate anions along the 1D chains of $[Mn(salpn)NCS]_n$ in 2. Hydrogen atoms have been omitted for clarity. Thermal ellipsoids are represented at 50% probability level. Symmetry labels: (i) $-x, -y, z + 1/2$.

Table 4.5 Selected bond lengths (A) and angles (°) in $[Mn(salpn)NCS]_n$ (2)

Mn-O1	1.880(2)	Mn-N2	2.037(2)	Mn-N3	2.270(3)
Mn-O2	1.897(2)	Mn-N1	2.042(2)	Mn-S1#1	2.7737(11)
O1-Mn-O2	85.37(9)	N2-Mn-N1	95.10(9)	O1-Mn-S1#1	90.47(9)
O1-Mn-N2	173.20(8)	O1-Mn-N3	92.63(11)	O2-Mn-S1#1	95.80(8)
O2-Mn-N2	88.83(9)	O2-Mn-N3	95.13(10)	N2-Mn-S1#1	86.57(8)

Table 4.5 contd.

O1-Mn-N1	90.70(9)	N2-Mn-N3	91.43(10)	Nl-Mn-Sl#l	84.41(7)
O2-Mn-N1	176.06(8)	Nl-Mn-N3	84.84(10)	N3-Mn-Sl#l	168.84(7)

#1 $-x, -y, z + 1/2$

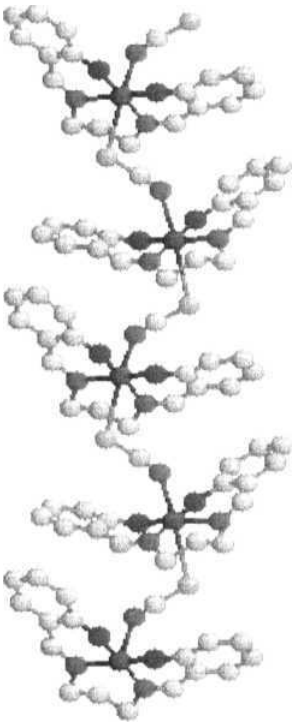

Figure 4.2 Perspective view of helical polynieric chains in 2. Colour code for atoms: blue, N; red, O; yellow, S; grey, C; dark grey, Mn.

chain formation. The Jahn - Teller axis around Mn(III) corresponds to the N3-Mn-S bond. The impact of this distortion on the magnetic properties is discussed later. The

inclination between the mean planes of the two halves of the SB ligand (excluding the methylene groups) is now 37.2(1)° as against 44.0(1)° in the azide complex..

4.2.2. Structure of **[Mn(salpn)NCS]$_2$** (1): The asymmetric unit of the dimer is shown in Figure 4.3. Here also, the salpn ligands adopt the equatorial coordination mode, however, the two halves of each salpn are now more coplanar than in the helical chain, the interplanar angle being 10.2(1)°. The thiocyanate ions remain terminal and N-bonded.

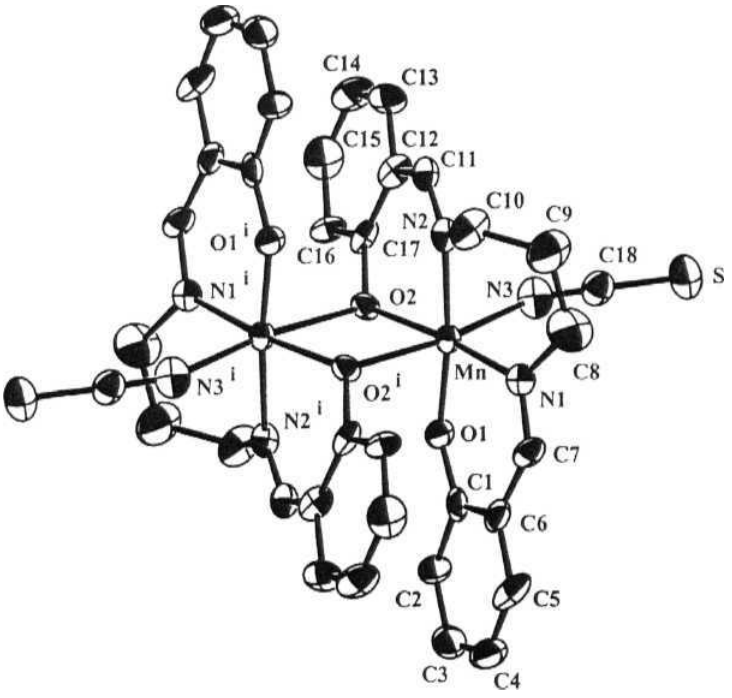

Figure 4.3 ORTEP view of the Mn(salpn)NCS dinuclear complex molecule in 1. Hydrogen atoms are omitted for clarity, and the thermal ellipsoids are represented at the 50% probability level. Symmetry labels:

Six coordination around the manganese atoms is completed by two highly unsymmetrical (Mn-0 1.923(3), 2.539(3) A) phenoxide bridges. The two halves of the dimer are related by a crystallographic inversion center. SCN-Mn-Obndge appears to be the Jahn-Teller elongation axis, even though the terminal thiocyanate ion is more strongly bound compared to the bridging thiocyanate in the polymer. The bridge angle $Mn\text{-}O_{bridge}\text{-}Mn'$ is 100.00(11)°, while the Mn-Mn' distance is 3.4406(11) A. The plane defining the MnO2Mn'O2' bridge makes an angle of 85.0(1)° with the equatorial coordination plane defined by the atoms, Mn, N1, N2, 01, and 02.

Table 4.6 Selected bond lengths and angles in $[Mn(salpn)NCS]_2$ (1).

Mn-O1	1.844(3)	Mn-02	1.923(3)	Mn-N1	2.024(4)
Mn-N2	2.025(4)	Mn-N3	2.154(5)	Mn-O2#1	2.539(3)
O1-Mn-N1	91.47(15)	O2-Mn-N1	168.77(14)	O1-Mn-O2	88.22(13)
O2-Mn-N2	87.31(14)	Nl-Mn-N2	92.04(15)	O1-Mn-N2	173.67(14)
O2-Mn-N3	99.58(15)	Nl-Mn-N3	91.61(16)	O1-Mn-N3	95.82(16)
N2-Mn-N3	89.35(16)	O1-Mn-O2#1	92.33(12)	O2-Mn-O2#1	80.01(12)
Nl-Mn-02#l	88.79(12)	N2-Mn-O2#1	82.48(13)	N3-Mn-O2#1	171.83(14)

#1 $-x, -y + 1, -z$

The uncoordinated S has a significant role in stabilizing the crystal structure. The most remarkable feature is the S - π(phenyl) interactions which connect the dimers into one dimensional chains running along the crystallographic *a*-axis (Figure 4.4). The

distance between the S atom and the centroid of the phenyl ring is 3.66 A, while the C-centroid-S angle is 90 ± 11° for the six ring C atoms. A search in the Cambridge Crystallographic Data base for metal complexes having N-coordinated NCS" ion interacting with the π-cloud of phenyl rings resulted in 57 hits. Restricting the C-centroid-S angle to 90 ± 2° reduces the number of structures to 14. As expected, S - *n* (phenyl) interaction is a "soft bond" being influenced by other crystal packing considerations. The four symmetry related chains are linked into a three dimensional network through C-H···S interaction, the S ••H distance being in the range 3.0-3.4 A.

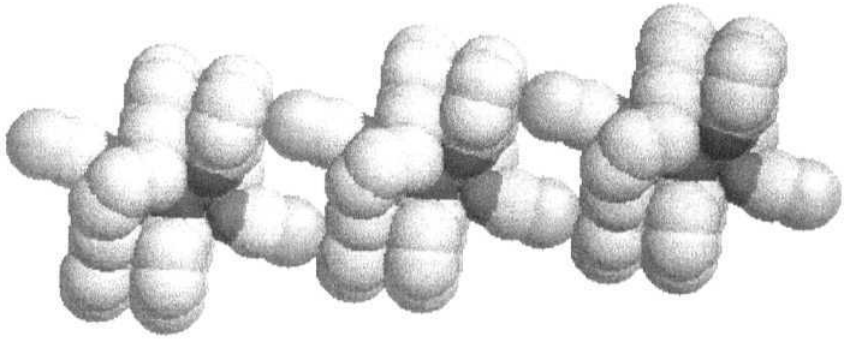

Figure 4.4 1-D chain of dimers linked by S···π(ring) interaction along the *a*- axis in 1. Colour code for atoms: blue, N; red, O; yellow, S; grey, C. The manganese atoms are hidden in this view.

4.2.3. Structure of Fe(salpn)(CH_3OH)NCS (3): The asymmetric unit is shown in Figure 4.5. In this case also, the salpn ligands adopt the equatorial coordination mode. Six coordination around Fe(III) is achieved by the coordination of NCS" ion and one solvent

CH3OH at the axial sites. The NCS" ion is terminal and N-bonded. The equatorial atoms Fe, N1, N2, 01 and 02 are nearly coplanar (rms devaiton, 0.09 A), the planarity being less than the that in $Fe(salpn)N_3$.[12] In $Fe(salpn)N_3$ the N3" ion is acting as μ-(1,1) bridge with the salpn ligand *cis*-octahedrally coordinated to Fe(III). The two halves of the ligand, excluding the methylene groups are also individually planar (rms deviation, 0.05 A), with the Fe atom deviating by 0.38 A and 0.51 A respectively. The angle between the two ligand planes is 28.75(10)° and is less than that in 2. The two Fe-O1 and Fe-O2

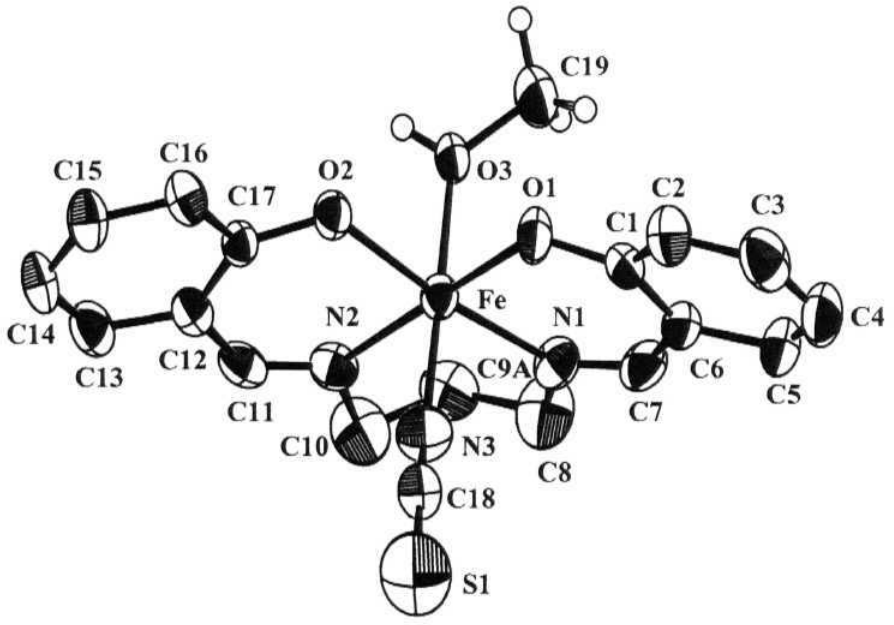

Figure 4.5 Ortep view of 3 with atom labeling. Atoms are shown as 50% thermal ellipsoids. Ring hydrogens have been omitted for clarity. Only one of the disordered C9 atom is shown.

distances are equal as in 1. In contrast to 1 and 2, the two Fe-N equatorial distances are also equal and shorter than the axial Fe-N bond (Table 4.7). However, the axial Fe-N distance is comparable to that observed in $Fe(salpn)N_3$. The uncoordinated S has a weak interaction with the C of the -C=N (S···C7 = 3.686(4) A) which connects the monomeric units into a polymeric chain (Figure 4.6). The methanolic hydrogen is involved in hydrogen bonding with a symmetry related phenoxide 02 (03 ••• O2#2 = 2.681 (4) A).

Table 4.7 Selected bond lengths and angles for $Fe(salpn)(CH_3OH)NCS$ (3).

Fe-O1	1.912(3)	Fe-N3	2.034(4)	Fe-N1	2.149(3)
Fe-02	1.944(2)	Fe-03	2.136(3)	Fe-N2	2.155(3)
O1-Fe-O2	94.31(10)	N3-Fe-O3	176.73(12)	O1-Fe-N2	179.14(10)
O1-Fe-N3	92.31(13)	O1-Fe-N1	87.97(12)	O2-Fe-N2	86.49(11)
O2-Fe-N3	96.32(12)	O2-Fe-N1	168.72(11)	N3-Fe-N2	87.93(13)
O1-Fe-O3	90.66(11)	N3-Fe-N1	94.63(13)	O3-Fe-N2	89.09(11)
O2-Fe-O3	84.82(11)	O3-Fe-N1	84.10(11)	Nl-Fe-N2	91.19(13)

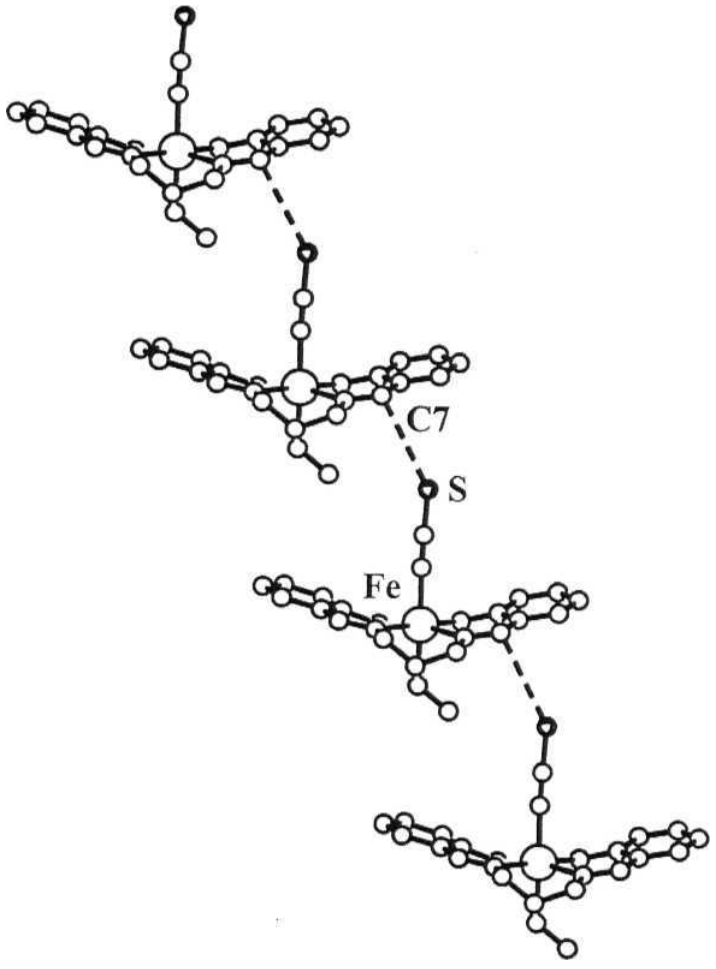

Figure 4.6 1-D Chain of monomeric 3 connected by weak S···C interactions (dotted lines).

4.3. Polymorphism and Optical Spectra: In case of 1 and 2 crystallization leads to one or the other polymorph or a mixture of the two depending upon the solvent and temperature. Acetonitrile and dichloromethane give only the dimer at both room temperature (RT) and low temperature (LT). The situation is similar in tetrahydrofuran, except that a small amount of polymer is also obtained at RT along with the dimer. Acetone produces a mixture at both temperatures, the amount of polymer being more at LT. Both methanol and ethanol give the dimer at RT and the polymer at LT. In the case of ethanol the LT product is contaminated with a small amount of the dimer. It turns out that the dimer is the preferred form at RT in all the solvents studied. Pure polymer is obtained only from methanol at LT. It is to be noted that even after complete evaporation of the solvent, there is no noticeable amount of dimer in the product obtained at LT from methanol, implying that dimer is kinetically not favoured at this temperature in this solvent. The two polymorphs 1 and 2 can be readily distinguished based on the IR absorption frequency corresponding to the N-C stretching vibration of the thiocyanate ion: 2043 cm^{-1} for dimer and 2068 cm^{-1} for polymer. The rest of the IR region (3000 - 400 cm^{-1}) is virtually identical for the two compounds (Figure 4.7). This is consistent with the general observation that the N-bonded thiocyanate ions have a lower N-C stretching frequency than the bridging thiocyanate.[31]

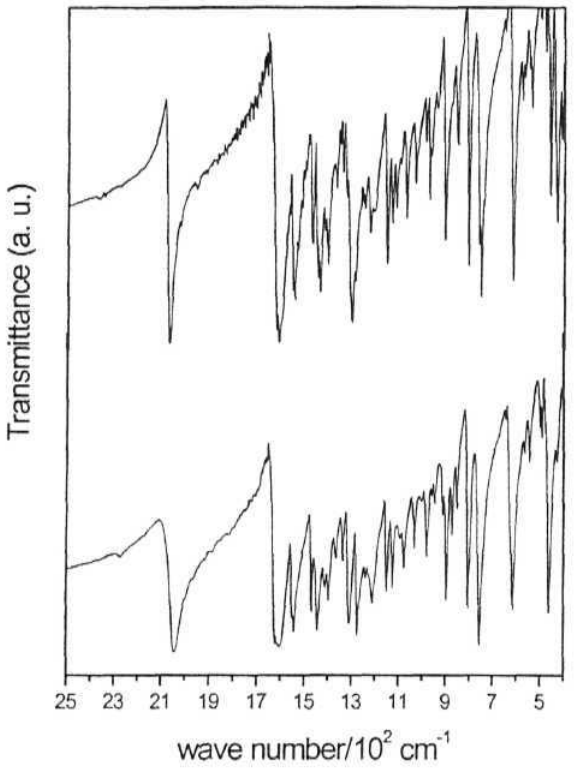

Figure 4.7 IR spectra of 1 (bottom) and 2 (top).

The **different** coordination environments in the two compounds is also reflected in the *d-d* absorption region: band maxima at 15690 cm'' and 16710 cm''' for 1; 16750 cm''' for 2(Figure 4.8a). The powder diffuse reflectance spectrum of 3 is presented in Figure 4.8b.

The solution spectra of the two polymorphs of Mn(III) in acetonitrile (Figure 4.9a) has several features and agree closely with the previously reported spectrum in aqueous solution:[32] 16750(220), 21100(1200), 25640(5000), 36100(17600) cm^{-1} ($Lmol^{-1}cm^{-1}$). The species present in solution is in all probability, solvent perturbed Mn(salpn)NCS. The bands at 21100 and 25640 cm^{-1} are probably due to ligand to metal charge transfer transition. The weak band at 16750 cm^{-1} is assigned to *d-d* transitions and probably includes in its envelope the transition from the split components of the ^5E state. The splitting is more prominent in the reflectance spectrum of 1 which has only weak axial interaction with the phenolate oxygen atoms. The solution spectra of 3 in acetonitrile (Figure 4.9b) also shows several features: 20200(1600), 31350(3700), 33900(3500), 38610(9100), 42730(15700), 46730(13900) cm^{-1}($Lmol^{-1}cm^{-1}$).

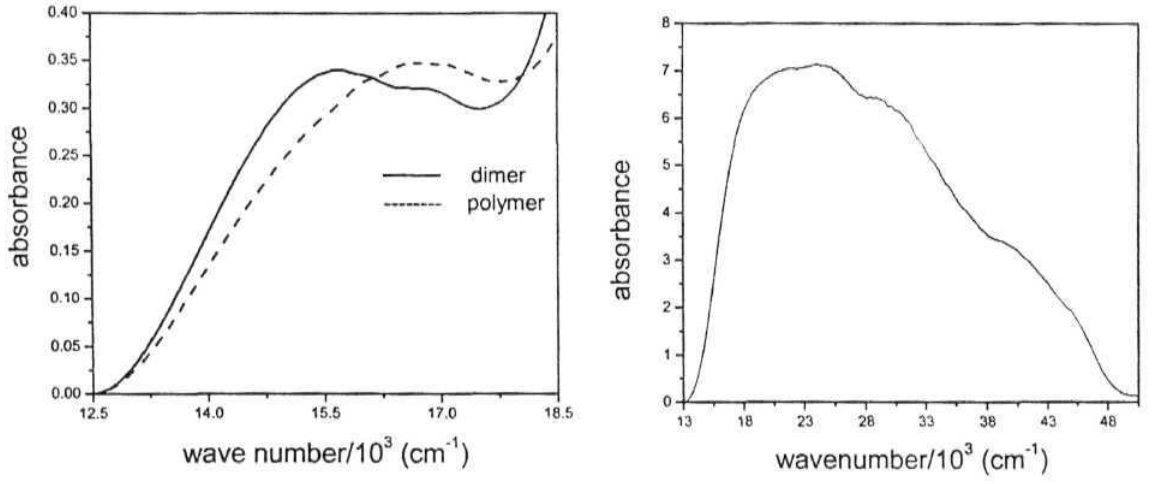

(a) (b)

Figure 4.8 Powder diffuse reflectance spectra of (a) dimeric and polymeric Mn(salpn)NCS and (b) monomeric Fe(salpn)(CH_3OH)NCS.

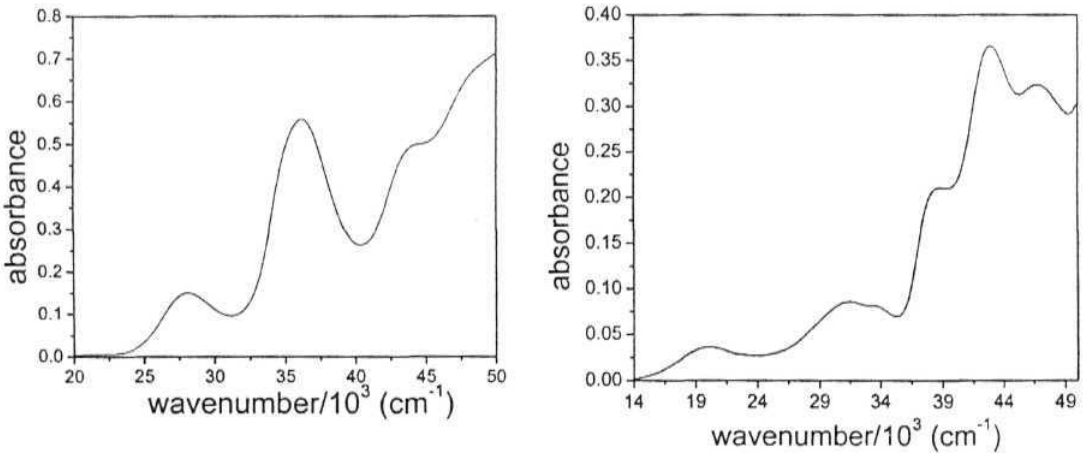

(a) **(b)**

Figure 4.9 Solution spectra of (a) **2** and (b) **3** in ACN.

4.4. **Magnetic Properties:** Magnetic susceptibility of 2 was measured between 300 K and 2 K. The results are represented in Figure 4.10 as the product $\chi_M T$ per Mn as a function of *T*. At 300 K, $\chi_M T$ =2.82 $cm^3 mol^{-1} K$. By itself this value which is lower than that for one isolated high spin Mn(III) indicates the presence of an antiferromagnetic coupling in the chain. This is confmned by the decrease of $\chi_M T$ as *T* decreases. At low temperature, an anomaly is observed in the $\chi_M T$ (see below). The data above 15 K are well fitted by the law for a chain of classical spins *S* = 2with *J* = -3.2 cm^{-1} and g = 1.99. (The *J* is defined in such a way that the singlet to triplet excitation energy for an antiferromagnetically coupled pair of *S* =1/2 ions is -*J*).

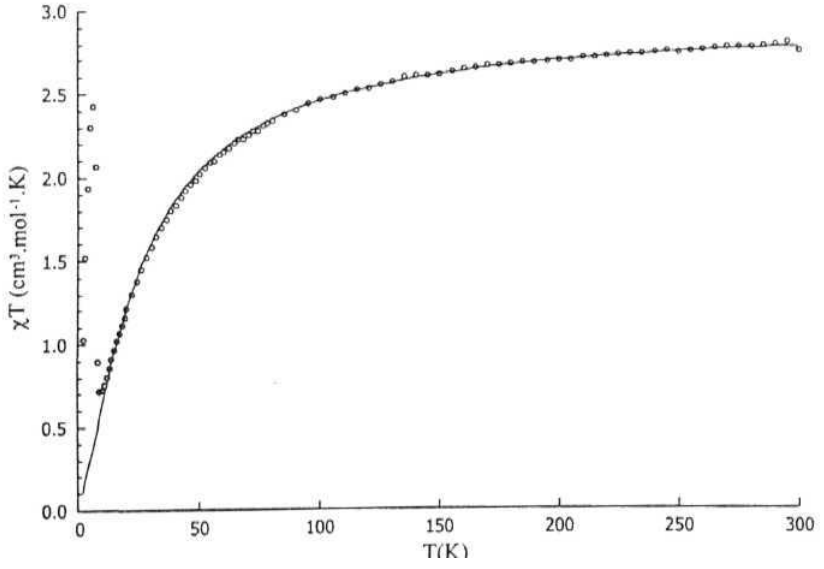

Figure 4.10 Product of the magnetic susceptibility per mole of manganese and temperature for the chain compound $[Mn(salpn)NCS]_n$

(dotted line). Solid line corresponds to the classical spin *S* - *2* chain model with g = 1.99, J = -3.2 cm^{-1} using data above 15 K.

The anomaly in $\chi_M T$ was found in fact to be related to a spin ordering phenomenon. First when we recorded the magnetization at 2 K versus magnetic field we obtained a curve (Figure 4.11) exhibiting two regimes. At low field, magnetization increases steeply with magnetic field; at higher field magnetization increases at a slower

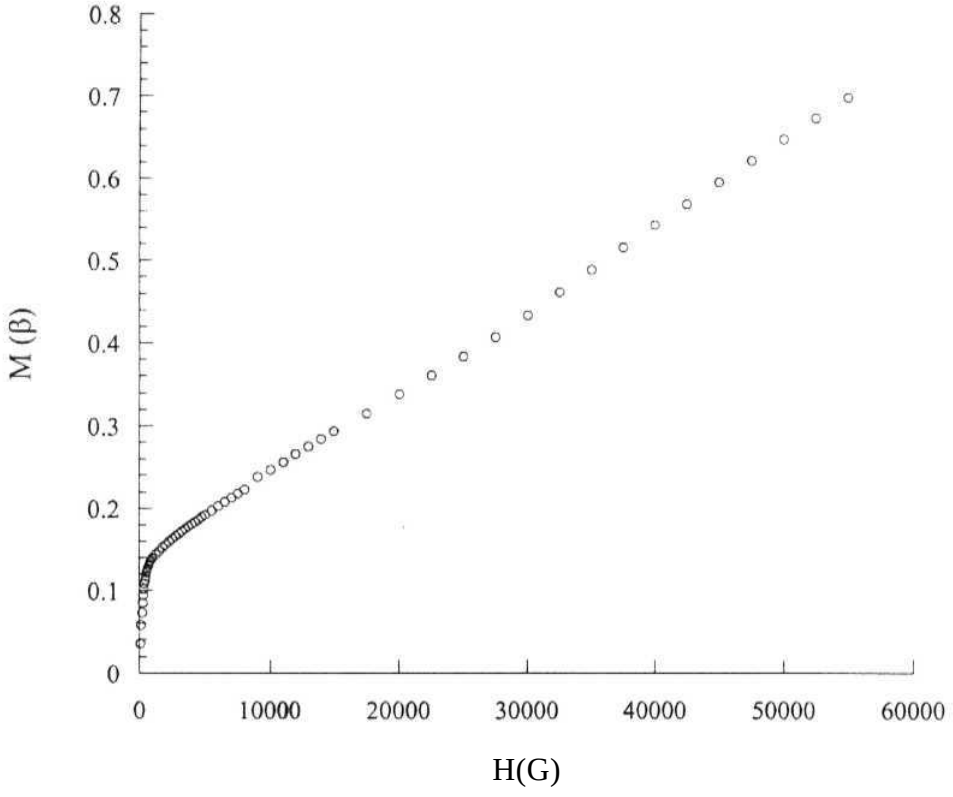

Figure 4.11 Magnetization per mole of manganese for 2 as a function of the magnetic field.

rate and in an almost linear fashion. This is strongly reminiscent of weak ferromagnetism.[33,34] An hysteresis (Figure 4.12) was detected in the ordered phase at 2 K with a coercive field of 2500 Oe.

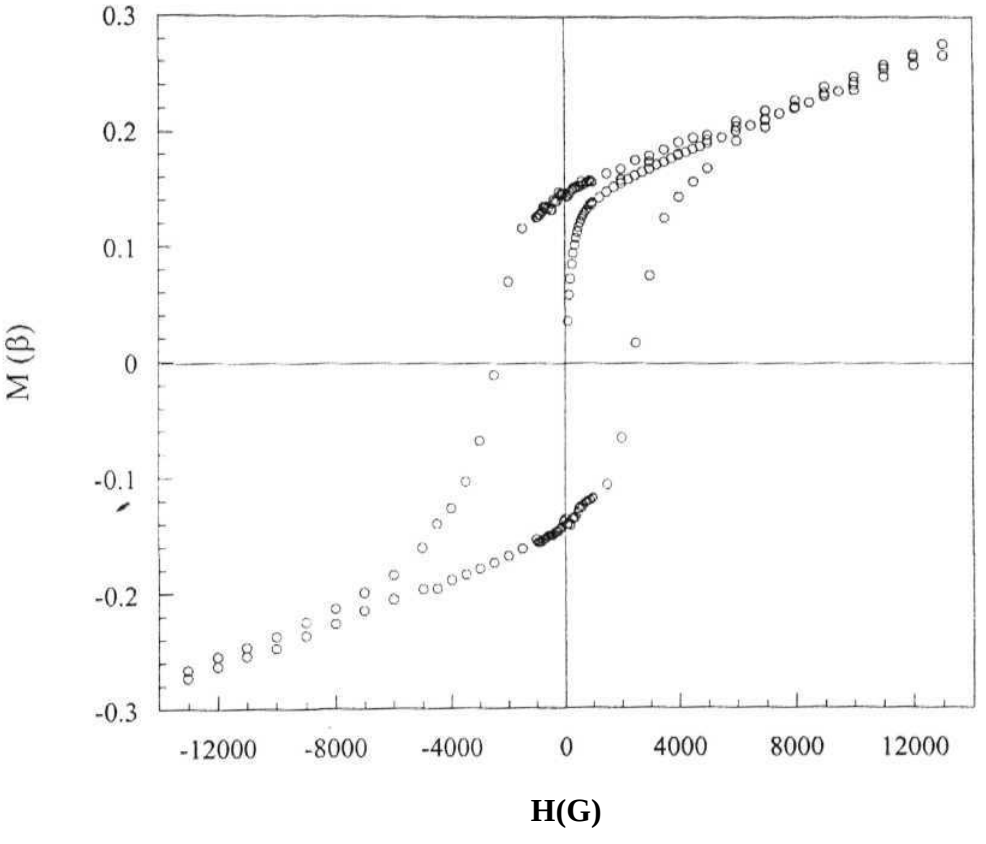

Figure 4.12 Hysteresis in the ordered phase of the chain compound $[Mn(salpn)NCS]_n$ at 2 K.

The phenomenology of the spin ordering was explored in detail (Figure 4.13) by measuring the zero field cooled (ZFC) and field cooled (FC) magnetization. The sample was cooled under zero field down to 4.5 K; at this temperature the field was set to 30 G and *T* was increased to 10 K. The sample was then cooled again under 30 G down to 4.5 K to get FC magnetization. As expected the FC curve is above the ZFC curve. The

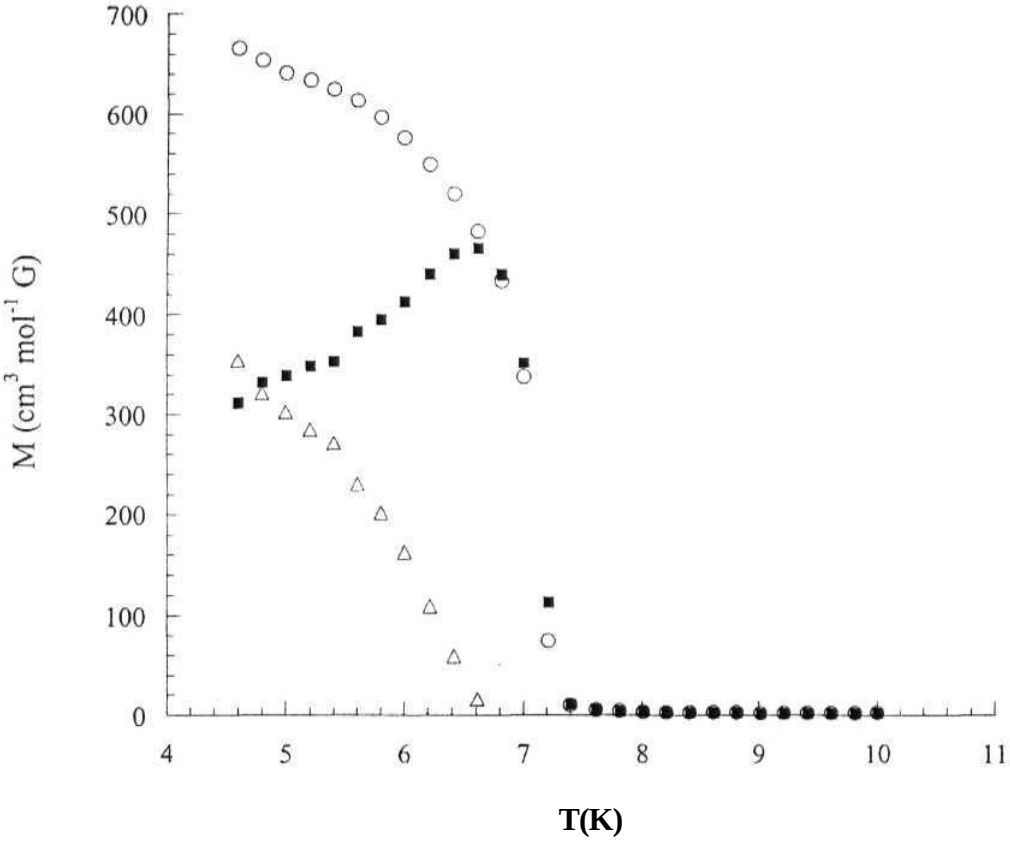

Figure **4.13** Temperature dependence of the magnetization per mole of manganese for the chain compound $[Mn(salpn)NCS]_n$ within a field of

30 G: (•) ZFC; (O) FC. The remnant magnetization was calculated as FC - ZFC (A).

difference is indicative of the remnant magnetization which is found to vanish at T_c = 6.8 K. It has to be noted that the saturation magnetization is only a fraction of the magnetization of a high spin Mn(III) (4 (3) as expected for weak ferromagnetism.

Magnetic susceptibility of 1 was measured between 300 K and 2 K. The results are represented in Figure 4.14 as the product $\chi_M T$ as a function of T. At 300 K the product $\chi_M T$ was found to be equal to 6.01 $cm^3 mol^{-1} K$ corresponding to the expected value for two isolated high spin Mn(III). No exchange coupling is detected from these data, the drop in $\chi_M T$ below ~5 K being due to zero field splitting.

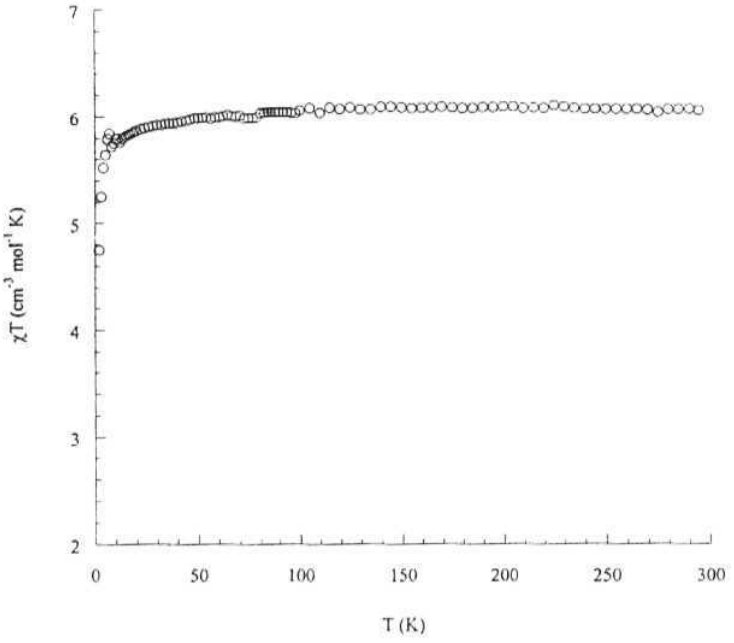

Figure 4.14 Product of the magnetic susceptibility per mole of manganese and temperature for the dimer compound $[Mn(salpn)NCS]_2$.

3 shows a room temperature magnetic moment of 6.26 BM, corresponding to high spin Fe(III). Variable temperature susceptibility studies are to be done.

4.5. Origin of the Weak Ferromagnetism of the Chain Compound: The anti ferromagnetic nature of the NCS* mediated coupling in the chain compound is quite clear from above. It is also well known that Mn(III) complexes exhibit a large anisotropy (typically D = -4 cm^{-1} for an elongation).[35]-[36] From the crystal structure it was observed that the Mn(III) ions are in an elongated environment with the Jahn-Teller (JT) elongation axis oriented towards the NCS" anion. The fourth unpaired electron is then in a d_{z^2} orbital with the z-axis along the JT axis. As a consequence the axial anisotropy energy

component must be negative which means the spins will tend to orient along the JT axis.[36]

It has to be remarked that the JT axis is tilted relative to the chain axis by 23° if we take the $Mn_nMn_{n+2}S_n$ angle, and by 34° if we take $Mn_nMn_{n+2}N_n$ angle. The canting angle *i.e.,* the angle between two successive spins *S,* and S_2 along the chain is calculated as follows. S_1 and S_2 are assumed to be along the respective bisecting vectors. The vectors are defined as,

$$\vec{u} = 0.5(\overrightarrow{Mn_1S_1} + \overrightarrow{N_1Mn_1})$$
$$\vec{v} = 0.5(\overrightarrow{Mn_2S_2} + \overrightarrow{N_2Mn_2})$$

where, S_1, Mn_1, N_1 and S_2, Mn_2, N_2 belong to adjacent (screw related) units in Figure 4. 2.

From the X-ray structure it is determined that,

$(\vec{u}, \vec{v}) = 55°$.

As a consequence, the uncompensated moment per Mn can be estimated as

$$M_s = M_0 \sin[(\vec{u}, v)/2] = 4\beta \sin(55/2) = 1.84\beta.$$

This is almost 10 times larger than the saturation moment which can be estimated from measurements at 2 K (Figure 4.11). It is assumed that the low value observed is due to a combination of antiferromagnetic coupling between chains with a canting effect. This would need further studies to be ascertained.

4.6. Conclusions

Two factors related to the formation of helical chain are the flexibility of the salpn ligand which allows considerable deviation from co-planarity of the two halves of this ligand (inclination angle, 37° in the thiocyanate complex, 44° in the azide complex[12]) and the Jahn-Teller elongation along the pseudohalide bridge. In the case of the present thiocyanate complex, a third factor comes into play, *viz.*, the expected low affinity of Mn(III) for coordination with S. This factor would contribute to the relative stability of the dimer in spite of the highly unsymmetrical nature of the phenolate bridges. An important feature of the dimer is the interaction between the phenyl ring and the free S atom of the thiocyanate ion. While such interactions are present in other crystal structures as shown by the data base search, the importance of this non-covalent interaction has not yet been fully appreciated. Although the preferred crystallization of the dimer from most solvents is certainly related to the above factors, it is not clear why the polymer is the kinetically preferred product from methanol and ethanol.

The thiocyanate mediated exchange along the helical chain is weakly antiferromagnetic. However, below 7 K a magnetic ordering with weak ferromagnetic coupling sets in. A magnetic anomaly was also observed in the Mn(III) azide chain complex although a different interpretation was given.[12] It is shown that, in the present case, the weak ferromagnetism arises through large magnetic anisotropy in Mn(III) and resultant spin-canting with respect to the chain direction.

The structure and magnetic properties of the dimer are at variance with the recently observed trends in phenolate bridged Mn(III) dimers of salen type Schiff base ligands. In the salen series[20] it was observed that, (i) in $Mn_2^{III}(SB)X_2$, when X = NCS" or Cl^- the *trans* $Mn\cdots O_{bridge}$ is long (3.44 - 3.76 A), whereas when X = OH_2, the Mn···

O_{bridge} is short (2.43 - 2.66 A) and (ii) short bridges result in stronger ferromagnetic interaction ($y \sim 3.0\ cm^{-1}$). In $Mn_2(salpn)_2(NCS)_2$, the $Mn\cdots O_{bridge}$ is short, but $J \sim 0$. There is no doubt that the $Mn\cdots O_{bridge}$ distance in the observed range is to some extent influenced by crystal packing considerations. However, the disagreement of the present dimer with the observed magneto-structural con-elation in the salen series is more difficult to explain. The net exchange parameter has contributions from several exchange pathways involving the four magnetic orbitals on each d^4 ion and these may be influenced by terminal ligands as well as bridge geometry. More phenolate bridged systems need to be studied to establish the correlations.

The formation of a monomeric complex with Fe(III) is contrary to the observations with Mn(III). As Fe(III) does not undergo Jahn-Teller distortion, salpn ligand in spite of being flexible could not stabilize a polymeric chain of Fe(III) as in the case of Mn(III). Also, the low affinity of Fe(III) towards S could not lead to a SCN" bridged dimer, thus forming only the monomeric complex. These observations are supported by the spectral studies where only one species is observed. The polymorphism seen in preliminary studies need to be investigated by finding the proper conditions for crystallization

4.7. References

(1) Vrieze, K.; van Koten, G. *Comprehensive Coordination Chemistry*; Wilkinson, G., Gillard, R. D. and McCleverty, J. A., Ed.; Pergamon Press: Oxford: England, 1987; Vol. 2, pp 225.

(2) Ribas, J.; Monfort, M.; Ghosh, B. K.; Cortes, R.; Solans, X.; Font-Bardia, M. *Inorg. Chem.* 1996, *35,* 864.

(3) Tuczek, F.; Bensch, W. *Inorg. Chem.* 1995, *34,* 1482.

(4) Escuer, A.; Vicente, R.; Goher, M. A. S.; Mautner, F. A. *Inorg. Chem.* 1995, *34,* 5707.

(5) Stults, B. R.; Marianelli, R. S.; Day, V. W. *Inorg. Chem.* 1975, *14*, 722.

(6) Ribas, J.; Monfort, M.; Diaz, C; Bastos, C; Solans, X. *Inorg. Chem.* 1994, *33,* 484.

(7) Mautner, A. F.; Goher, M. A. S. *Polyhedron* 1996, *15,* 1133.

(8) Cortes, R.; Pizarro, J. L.; Lezama, L.; Arriortua, M. I.; Rojo, T. *Inorg. Chem.* 1994, *33,* 2697.

(9) De Munno, D.; Poerio, T.; Viau, G.; Julve, M.; Lloret, F. *Angew. Chem. Int. Ed. Engl.* 1997, *36,* 1459.

(10) Wemple, M. W.; Adams, D. M.; Hagen, K. S.; Folting, K.; Hendrickson, D. N.; Christou, G. J. *Chem. Soc, Chem. Commun.* 1995, 1591.

(11) Li, H.; Zhong, Z. J.; Duan, C.-Y.; You, X.-Z.; Mak, T. C. W.; Wu, B. *Inorg. Chim. Acta.* **1998**, *271*, 99.

(12) Reddy, K. R.; Rajasekharan, M. V.; Tuchagues, J.-P. *Inorg. Chem.* 1998, *37,* 5978.

(13) Shen, H.-Y.; Liao, D.-Z.; Jiang, Z.-H.; Yan, S.-P.; Sun, B.-W.; Wang, G.-L.; Yao, X.-K.; Wang, H.-G. *Chem. Lett.* **1998,** 469.

(14) Zhang, K.-L.; Chen, W.; Xu, Y.; Wang, Z.; Zhong, Z. J.; You, X.-Z. *Polyhedron* **2001,** *20,* 2033.

(15) Gregson, A. K.; Moxon, N. T. *Jnorg. Chem.* **1982,** *21,* 586.

(16) Kennedy, B. J.; Murray, K. S. *Inorg. Chem.* **1985,** *24,* 1552.

(17) Mikuriya, M.; Yamato, Y.; Tokii, T. *Bull. Chem. Soc. Jpn.* **1992,** *65,* 1466.

(18) Kolawole, G. A. *Synth. React. Inorg. Met.-Org. Chem.* **1993,** *23,* 907.

(19) Agarwal, D. D.; Bhatnagar, R. P.; Jain, R.; Srivastava, S. *J. Chem. Soc, Perkin Trans.* 2 **1990,989.**

(20) Miyasaka, H.; Clerac, R.; Ishii, T.; Chang, H.-C.; Kitagawa, S.; Yamashita, M. *J. Chem. Soc, Dalton Trans.* **2002,** 1528.

(21) Reddy, K. R. *Research Report: C. S. 1. R. Associateship:* Hyderabad, 1996.

(22) North, A. C. T.; Phillips, D. C; Mathews, F. S. *Acta Cryst.* **1968,** *A24,* 351.

(23) Walker, N.; Stuart, D. *Acta Crystallogr.* **1983,** *A39,* 153.

(24) Sheldrick, G. M. *Ada Crystallogr.* **1990,** *A46,* 467.

(25) Sheldrick, G. M. *SHELXS97 and SHELXL 97;* University of Gottingen: Germany, 1997.

(26) Burnett, M. N.; Johnson, C. K. *ORTEP-III: Oak Ridge Thermal Ellipsoid Plot Program for Crystal Structure Illustrations*; Oak Ridge National Laboratory Report ORNL-6895: Tennessee, USA, 1996.

(27) Sayle, R. *RasMol V2.6*: Stevenage, Hertfordshire, U.K., 1995.

(28) Kraus, W.; Nolze, G. *Powder Cell for Windows version 2.3;* Federal Institute for Materials Research and Testing: Berlin, Germany, 1999.

(29) Fisher, M. E. *Am. J. Phys.* **1964,** *32,* 343.

(30) Datta, R. L.; Syamal, A. *Elements of Magnetochemistry;* S. Chand Co. Ltd.: New Delhi (India), 1982.

(31) Nakamoto, K. *Infrared and Raman Spectra of Inorganic and Coordination Compounds;* 3 ed.; John Wiley & Sons, Inc.: New York, 1977, pp 270.

(32) Ashmawy, F. M; Mc Auliffe, C. A.; Parish, R. V.; Tames, J. *Inorg. Chim. Acta.* **1985,** *103,* 133.

(33) Carlin, R. L.; Van Duyneveldt, A. J. *Magnetic Properties of Transition Metal Compounds;* Springer-Verlag, Inc.: New York, 1977; Vol. 2, pp 184.

(34) Bakalbassis, E.; Bergerat, P.; Kahn, O.; Jeannin, S.; Jeannin, Y.; Dromzee, Y.; Guillot, M. *Inorg. Chem.* **1992,** *31,* 625.

(35) Barra, A.-L.; Gatteschi, D.; Sessoli, R.; Abbati, G. L.; Cornia, A.; Fabretti, A. C; Uytterhoeven, M. G. *Angew. Chem. Int. Ed. Engl.* **1997,** *36,* 2329.

(36) Gerritsen, H. J.; Sabisky, E. S. *Phys. Rev.* **1963,** *132,* 1507.